PCCP

Cite this: *Phys. Chem. Chem. Phys.*, 2012, **14**, 5581–5587

www.rsc.org/pccp

PAPER

In situ X-ray Raman spectroscopy of $LiBH_4$†

Piter S. Miedema,*[a] Peter Ngene,[a] Ad M. J. van der Eerden,[a] Tsu-Chien Weng,[b] Dennis Nordlund,[b] Dimosthenis Sokaras,[b] Roberto Alonso-Mori,[c] Amélie Juhin,[a] Petra E. de Jongh[a] and Frank M. F. de Groot*[a]

Received 16th December 2011, Accepted 27th February 2012
DOI: 10.1039/c2cp24025d

X-Ray Raman Spectroscopy (XRS) is used to study the electronic properties of bulk lithium borohydride ($LiBH_4$) and $LiBH_4$ in porous carbon nano-composites ($LiBH_4$/C) during dehydrogenation. The lithium (Li), boron (B) and carbon (C) K-edges are studied and compared with calculations of the starting material and intermediate compounds. Comparison of the B and C K-edge XRS spectra of the as-prepared samples with rehydrogenated samples shows that the B and C electronic structure is largely regained after rehydrogenation. Both Li and C K-edge spectra show that during dehydrogenation, part of the Li intercalates into the porous carbon. This study shows that XRS in combination with calculations is a promising tool to study the electronic properties of nano-crystalline light-weight materials for energy storage.

1 Introduction

A X-Ray Raman spectroscopy

The X-ray spectra of light elements, such as lithium (Li), boron (B) and carbon (C), occur in the soft X-ray energy range at, respectively, 60 eV, 180 eV and 280 eV. X-Ray Absorption Spectroscopy (XAS) can be measured in transmission, electron yield or fluorescence yield. Due to the path lengths of soft X-rays, transmission X-ray absorption measurements in the energy range of 50 to 250 eV are as yet impossible. Above 250 eV, transmission X-ray microscopy can be performed at ambient pressure[1] using specialized nano-reactors.[2] The electron yield mode can as yet only be performed at the mbar pressure range.[3] Fluorescence yield probes deeper into the sample, but this probe has very low yield for soft X-ray energies and suffers from saturation effects in concentrated systems.[4]

X-Ray Raman Spectroscopy (XRS) measures the energy loss of a hard X-ray beam and as such it is a technique that can retain the experimental advantages of hard X-ray measurements (deeper probing depth implying more realistic samples, less beam damage, experiments in a gas environment), while revealing the information equivalent to the soft X-ray absorption spectra.[5,6] Thus, XRS on the K-edge of the light-weight elements can circumvent the problems related to soft X-rays. Initially, the low cross-section of XRS made this technique impractical, but intense new X-ray facilities and improvements in X-ray optics helped XRS to become an interesting spectroscopic tool.[7] The difference between XRS and XAS is the transition operator. In XAS the electronic transition can be approximated as a dipole transition, while for XRS also higher order transitions (quadrupole, *etc.*) are allowed, depending on the *q*-vector, related to the angle between incident and scattered X-rays. At low values for *q* as used in our experiment only dipole transitions are allowed. Note that resonant X-ray Raman Spectroscopy, also known as Resonant Inelastic X-ray Scattering (RIXS), would even give more electronic information, but because the B and Li K-edges are at 60 eV and 180 eV soft X-ray edges, *in situ* RIXS experiments cannot be performed.

In this study we show experimental XRS data on the B K-edge and Li K-edge of the hydrogen storage material $LiBH_4$ and compare the XRS with calculations.

B Background on (nanoconfined) $LiBH_4$

$LiBH_4$ is a complex metal hydride that has recently attracted much attention as a potential material for onboard hydrogen storage in cars due to its hydrogen content of 18.5 wt%. When heated, it decomposes into LiH and B in three intermediate steps, releasing 13.8 wt% hydrogen.[8] The reaction pathway and intermediate decomposition products have been the subject of a number of recent investigations.[9–11] The intermediate products are generally amorphous and their formation depends on experimental parameters such as temperature, heating rate and the carrier gas. Kang *et al.* proposed that LiBH and LiB

[a] *Department of Inorganic Chemistry and Catalysis, Debye Institute for Nanomaterials Science, Utrecht University, Universiteitsweg 99, 23584 CG Utrecht, The Netherlands. E-mail: p.s.miedema@gmail.com, f.m.f.degroot@uu.nl*
[b] *Stanford Synchrotron Radiation Lightsource, SLAC National Accelerator Laboratory, 2575 Sand Hill Road, Menlo Park, CA 94025, USA*
[c] *Linear Coherent Light Source, SLAC National Accelerator Laboratory, 2575 Sand Hill Road, Menlo Park, CA 94025, USA*

† Electronic supplementary information (ESI) available: XRS spectra of Li_4SiO_4 and BN and calculation details on different studied systems and calculated B and Li K-edges of reference systems and intermediates $Li_2B_{12}H_{12}$, LiB, LiBH and LiH. See DOI: 10.1039/c2cp24025d

are the intermediate phases.[12] The reaction would in that case proceed according to:

$$LiBH_4 \rightleftarrows LiBH + 3/2H_2 \rightleftarrows LiB + 2H_2$$

Ohba *et al.* predicted from calculations that monoclinic $Li_2B_{12}H_{12}$ is formed as the intermediate compound during dehydrogenation of $LiBH_4$ and subsequent rehydrogenation.[13] In their search for stable intermediates, no compound or crystal structure more stable than monoclinic $Li_2B_{12}H_{12}$ was found.[13] They propose the following reaction:

$$LiBH_4 \rightleftarrows 1/12Li_2B_{12}H_{12} + 5/6LiH + 13/12H_2$$
$$\rightleftarrows LiH + B + 3/2H_2$$

Orimo *et al.* published experimental XRD and Raman spectra at different temperatures, which are in agreement with the proposed intermediate $Li_2B_{12}H_{12}$.[9] Nuclear Magnetic Resonance (NMR) spectroscopy experiments by Hwang *et al.* gave further confirmation of the formation of $Li_2B_{12}H_{12}$ during the decomposition of $LiBH_4$.[10] Other literature suggests that $Li_4B_4H_{10}$ ($LiBH_{2.5}$) could be a possible intermediate decomposition product of $LiBH_4$. Many other stable boron–hydrogen complexes are known, such as B_4H_8 and B_4H_{10}.[11]

The rates of hydrogen release and uptake in $LiBH_4$ can be improved by confinement in nanoporous carbon which sometimes also results in a change in the stability and decomposition pathway of the compound.[14–16] At the moment the exact role of the nanoconfinement and the carbon in improving the hydrogen sorption properties of $LiBH_4$ is not well understood. Nanoconfined $LiBH_4$ and other complex hydrides often lack long-range crystallinity and therefore cannot be characterized using conventional techniques like XRD, and due to weak scattering of electrons by the light elements Li and B, $LiBH_4$ cannot be reliably imaged with TEM.

In this study, we investigate the suitability of XRS as a tool to study the chemical and structural transformations that occur in Li, B and C during the dehydrogenation and after subsequent rehydrogenation of both bulk $LiBH_4$ and nanoconfined $LiBH_4$.

2 Experimental and theoretical section

A Experimental section

A.1. Samples and sample preparation. $LiBH_4$ powder (95% pure) was purchased from Acros-organics. Lithium metal foil (99.9% pure) and BN powder (98% pure) were purchased from Sigma-Aldrich and Li_4SiO_4 powder (99.9% pure) was purchased from Alfa Aesar. The graphite and porous carbon (High surface area graphite: HSAG-500, pore volume 0.65 $cm^3\ g^{-1}$, broad pore size distribution but majority pore size 2–3 nm) were provided by Timcal Switzerland. The nanoconfined samples were prepared by melt-infiltration of 25 wt% $LiBH_4$ into the porous carbon ($LiBH_4$/C) under a hydrogen pressure of 100 bar at a temperature of 295 °C.[17] Sample preparation and handling was conducted in an argon filled glove-box (typically <1 ppm of oxygen and moisture) to avoid contamination. The prepared samples were packaged and shipped to the USA in an air tight container. This air-tight container was made of steel and was introduced into the argon filled glove-box. The samples were put in small bottles and closed and put in the air-tight container creating a double protection against oxygen and vapour contamination. This air tight container was brought in a nitrogen-filled glove box at the Stanford Synchrotron Radiation Light Source (SSRL) and opened inside the glove box.

A.2. *In situ* cell. An *in situ* XAS cell, developed by our group for measurements of samples under reaction conditions at elevated temperatures and flowing or static gas atmospheres, was used.[18,19] This cell was originally developed for transmission XAS and for fluorescence yield XAS.

In this original reactor cell, the signal was disturbed by scattered and fluorescence light of the interior wall of the *in situ* cell. This disturbance can especially occur for samples containing iron and other metals from the transition metal group. To circumvent this disturbance, the application of a gold coating of ~40 micron thickness was used on both the interior wall of the *in situ* cell as well as the cylinder with the sample holder. This created a reactor cell with a completely covered golden interior. The upper part of the cell accommodates tubes for liquid nitrogen feed to cool the sample, connections for a furnace and a thermocouple. On top a reservoir for liquid nitrogen can be placed. The reaction chamber usually is at ambient pressure and can be flushed with gases. The cell is double-walled and can be water-cooled to prevent the windows to be overheated and to prevent condensation of water vapor on the windows during cooling of the cell.

The sample holder has a slit (3 × 12 mm) for a pressed sample wafer. The *in situ* cell can be used for transmission measurements, for fluorescence and for XRS. The sample holder is placed perpendicular or at an angle (35° to 60°) to the incoming beam. The fluorescent radiation emitted by the sample is measured with a solid state detector perpendicular to the direction of the incident beam, through the large window in front. Both the entrance flanges and fluorescence window are sealed by Kapton foil (25 μm).

For our purpose of XRS experiments, the position of the *in situ* cell has been optimized for a large solid angle of the (high momentum transfer q) inelastic scattered X-rays through a large exit window (see Fig. 1). The exit window is wide enough to record the high and low q inelastic scattered X-rays without changing the cell position.

For the XRS measurements, the samples were pressed in the sample holder which was placed in the air tight *in situ* cell in a nitrogen filled glove box available at the Stanford Synchrotron Radiation Light Source (SSRL). The whole *in situ* cell was then taken out of the glove box and taken to the beam line for measurements.

A.3. X-Ray Raman spectroscopy measurements. Lithium (Li), boron (B) and carbon (C) K-edge XRS spectra were collected at SSRL beamline BL6-2 ES2. The *in situ* cell was mounted on a pre-constructed plate, so that the *in situ* cell was every time at exactly the same angle with reference to the beam. The XRS scans were performed using the inverse energy scan technique:[20,21] the scattered photons are analyzed at a fixed energy and the energy transfer is controlled by tuning

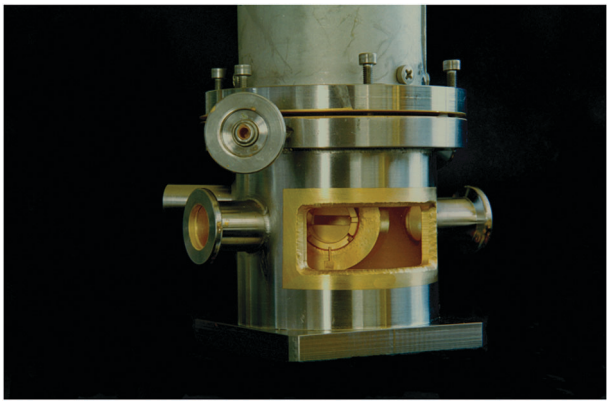

Fig. 1 Picture of the lower part of the *in situ* setup.

the incident photon energy. The incident photon energy was selected with a Si(311) monochromator. The XRS spectra were collected by scanning the incident beam energy relative to the fixed analyzer energy of 6462.20 eV with a resolution of 0.3 eV. The XRS spectra were measured using 25 detector crystals with an average q-vector of 1.3 atomic units, implying essentially pure dipole transitions. The XRS spectra are plotted as normalized scattered intensity *versus* energy loss (incident energy minus elastic energy). During the XRS measurements, the cell was under a nitrogen atmosphere.

Hexagonal boron nitride powder (h-BN), lithium metal (Li (metal)) foil and Li_4SiO_4 powder are the reference XRS measurements that can be compared with literature XAS, XRS and Electron Energy Loss (EELS) spectra. In addition, for Li metal and h-BN XAS calculations were performed (see theoretical section). The XRS of h-BN, Li_4SiO_4 and the XAS calculation of BN are given in the ESI†, Fig. S1–S3.

The Li and B K-edge XRS of $LiBH_4$ powder is measured at room temperature (RT), at 200 °C, and then at RT after cooling down. XRS of the $LiBH_4$/C is measured at RT, at 200 °C, at 450 °C and again at RT after cooling down. The B and Li K-edges of bulk $LiBH_4$ and $LiBH_4$/C (as synthesized, dehydrogenated and rehydrogenated) were compared with XAS calculations (see theoretical section). C K-edge XRS of some of the samples have been measured at RT before and after dehydrogenation and after rehydrogenation. Note that the rehydrogenated samples are not identical to the samples as prepared and during dehydrogenation. The rehydrogenated samples were prepared by melt infiltration, dehydrogenated and rehydrogenated *ex situ*. The conditions for the rehydrogenation were 50 bar H_2 pressure at 325 °C for three hours.

B Theoretical section

Li- and B-K edge XAS calculations were performed for the following model compounds: LiB, LiBH and $LiBH_4$,[12] BN,[22] Li(metal), B(tetragonal), and B(hexagonal),[23] LiH,[24] $Li_2B_{12}H_{12}$,[13,25] and B_2O_3.[26] Details about the crystal structures are given in Table S1 of the ESI.† First principles calculations were performed using the QUANTUM-ESPRESSO first principles total-energy code.[27] The code uses plane waves and periodic boundary conditions. The XAS spectra are obtained in two steps: first the charge density is obtained self-consistently using the PW package of the QUANTUM-ESPRESSO distribution[27] (self-consistent field (scf) calculation), then the XAS spectrum is computed in a continued fraction approach using the XSPECTRA package.[28–30] We use the General Gradient Approximation. For Li and B norm-conserving pseudo-potentials with two projectors per channel are used, and for O, N, and H, ultra-soft pseudopotentials are used. The electronic configurations are the following: $1s^1$ for H, $2s^2\ 2p^4$ for O, $2s^2\ 2p^3$ for N, $2s^2\ 2p^{0.9}$ for B, $2s^{0.9}\ 2p^0$ for Li, $2s^2\ 2p^1$ for B* (absorbing boron atom with a 1s core-hole) and $2s^1\ 2p^0$ for Li* (absorbing lithium atom with half a 1s core-hole), all without nonlinear core correction. For Li* only a half core hole is considered, since there are in total three electrons in lithium and therefore a full core hole could collapse the Li* pseudopotential.

The effect of the 1s core hole is taken into account using a supercell whose size is chosen large enough to avoid interaction between neighboring core-holes (ESI†, Table S1) and where the absorbing atom carries a core-hole. Since it is debated whether XAS calculations for K-edges of light-elements lower than carbon shall be done with or without the 1s core-hole,[31–33] calculations were performed with (full or half) or without the core-hole on the absorbing atom. The absorption cross section was computed in the electric dipole approximation. The isotropic XAS spectrum was calculated according to the formula given by Brouder,[34] depending on the symmetry of the crystal. Convergence of the XAS spectra is reached for the following set of parameters: a 60 Ry energy cutoff for the plane-wave expansion, a 600 Ry cutoff for the charge density, a Monkhorst–Pack k-point grid which depends on the system (see ESI†, Table S1) for the self-consistent electronic potential calculation and an $8 \times 8 \times 8$ k-point grid for the absorption cross-section calculation. For the convolution of the XAS spectra we used a constant broadening parameter of 0.3 eV both at the Li and B K edge. The calculated spectra were aligned to experiment.

In this paper only the results of the XAS calculations of Li(metal), B_2O_3 and $LiBH_4$ are shown. Results of the XAS calculations of other crystal structures are given in the ESI† in Fig. S3–S6.

3 Results and discussion

A Reference systems

In Fig. 2A the B K-edge XRS for bulk $LiBH_4$ and for the $LiBH_4$/C are shown. Both the B K-edge spectra of bulk $LiBH_4$ and $LiBH_4$/C have a main peak at 191.7 eV. The spectrum of $LiBH_4$/C as prepared has a second peak at 194 eV, which cannot be directly attributed. This peak might originate from oxidic boron, such as $LiBO_2$ or B_2O_3, which has an intense peak at about 194 eV.[35–37]

In Fig. 2C XAS calculations for crystals of $LiBH_4$ (bottom lines) and B_2O_3 (top lines) are shown. The XAS of the $LiBH_4$ with core-hole (solid line) agrees with the experimental XRS in Fig. 2A. The XAS calculation for B_2O_3 with core-hole agrees with other published XAS and EELS spectra.[36–38] Also XAS calculations for proposed intermediate compounds, including $Li_2B_{12}H_{12}$ and LiBH, were performed but none of the calculations resembles the experimental XRS spectrum. The calculated XAS of the intermediate compounds are given in the ESI†, Fig. S3–S6.

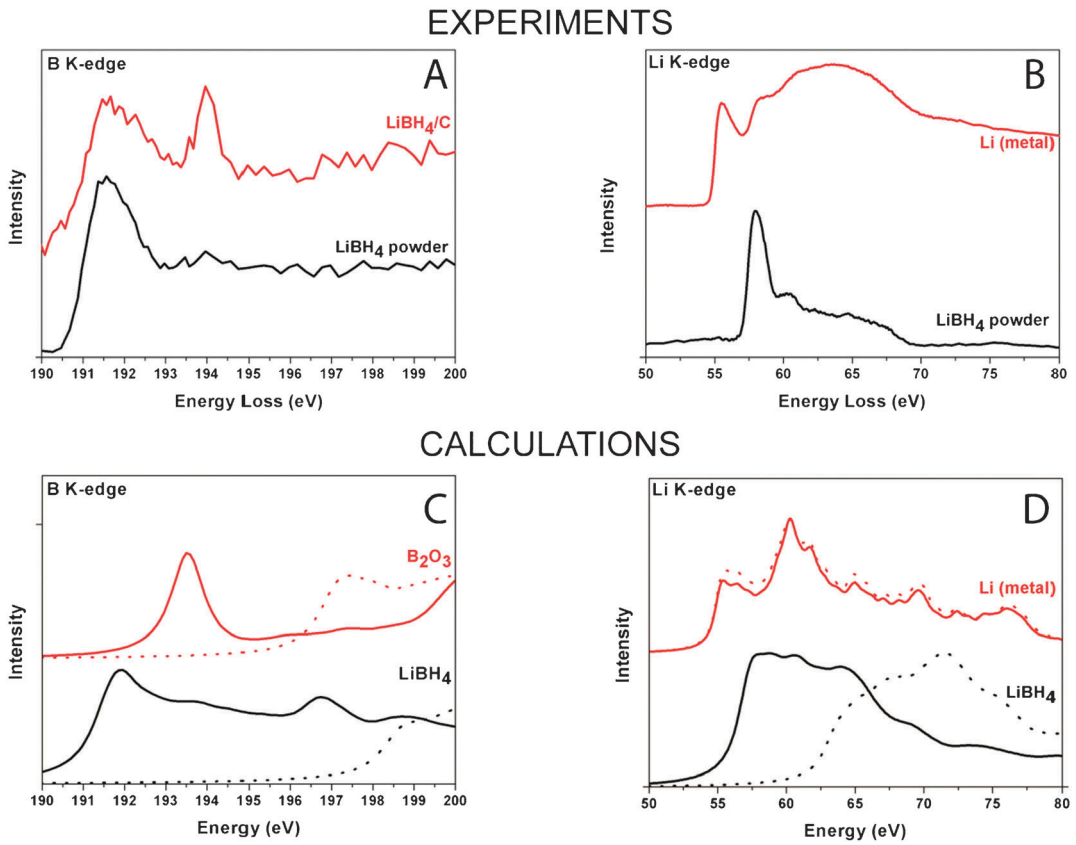

Fig. 2 (A) B K-edge XRS on bulk $LiBH_4$ powder (bottom line) and $LiBH_4$/C as prepared ($LiBH_4$/C, line on top); (B) Li K-edge XRS on bulk $LiBH_4$ powder (bottom line) and lithium metal foil (Li (metal), line on top); (C) XAS calculations on the B K-edge for $LiBH_4$ (bottom lines) and for B_2O_3 (lines on top); (D) XAS calculations on the Li K-edge for $LiBH_4$ (bottom lines) and for lithium (Li (metal), lines on top). For all calculations in C and D, the solid lines are the calculations with (half) core-hole and the dotted lines are the calculations without core-hole.

For the Li K-edge XRS of lithium metal foil (Li (metal) and $LiBH_4$ bulk powder the XRS is shown in Fig. 2B. The XAS calculation for the Li K-edge of $LiBH_4$ is shown in Fig. 2D. The XAS calculations with a half core-hole for the Li K-edge of $LiBH_4$ (Fig. 2D, bottom solid line) reproduce the XRS peaks at the same energies, but the intensity of especially the first peak in XRS is lower in the XAS calculations. This could be an effect of the background subtraction of the experimental XRS of $LiBH_4$, which could lead to intensity differences with the calculated XAS.

For all the B and Li K-edge XAS calculations in Fig. 2, it is clear that the peaks of XAS shift to lower energy when there is a core-hole used in the calculation. In addition, the peaks are narrower and more pronounced in cases when the calculation includes a core-hole. It was claimed that XAS calculations on B K-edges with full core-hole are in better agreement with experimental results than calculations without core-hole.[39–41] In this study this claim is confirmed. For Li K-edges we can state that XAS calculations with half core-hole compare better with experimental XRS results than XAS calculations without core-hole.

B Bulk $LiBH_4$ during dehydrogenation

The experimentally obtained XRS spectra of the Li and B K-edge for $LiBH_4$ and $LiBH_4$/C at different temperatures during dehydrogenation are shown in Fig. 3. Fig. 3A and C are the B K-edge XRS spectra and Fig. 3B and D the Li K-edge XRS of bulk $LiBH_4$ and $LiBH_4$/C respectively. In the Li K-edge XRS for bulk $LiBH_4$ (Fig. 3B), there are no significant changes between the spectrum at room temperature, the spectrum at 200 °C and the spectrum after heating and cooling down to room temperature, although one could argue that the features between 60 eV and 70 eV become less pronounced. The B K-edge spectra for bulk $LiBH_4$ in Fig. 3A show an extra peak at 194 eV upon heating. The first peak, corresponding to $LiBH_4$, does not disappear but coexists with the new peak at 194 eV. Higher temperatures than 200 °C were not used for the bulk $LiBH_4$ powder sample to prevent the $LiBH_4$ from melting and coating the interior of the *in situ* cell.

C Nanoconfined $LiBH_4$ during dehydrogenation

For the nanocomposite $LiBH_4$/C at room temperature, two peaks are present in the B K-edge spectrum (Fig. 3C, bottom line). These are the same peaks as in the B K-edge spectra of the bulk $LiBH_4$ powder at 200 °C and bulk $LiBH_4$ powder after heating and cooling down to room temperature (RT (after), top line) in Fig. 3A. The nanoconfined structure of $LiBH_4$/C is therefore supposed to be close to that of the bulk $LiBH_4$ structure. For $LiBH_4$/C at 175 °C, the peak at 191.5 eV almost disappears. At higher temperatures the 191.5 eV peak disappears completely. Only the peak at approximately 194 eV remains. This peak is attributed to "B_2O_3-like" materials, so it seems that

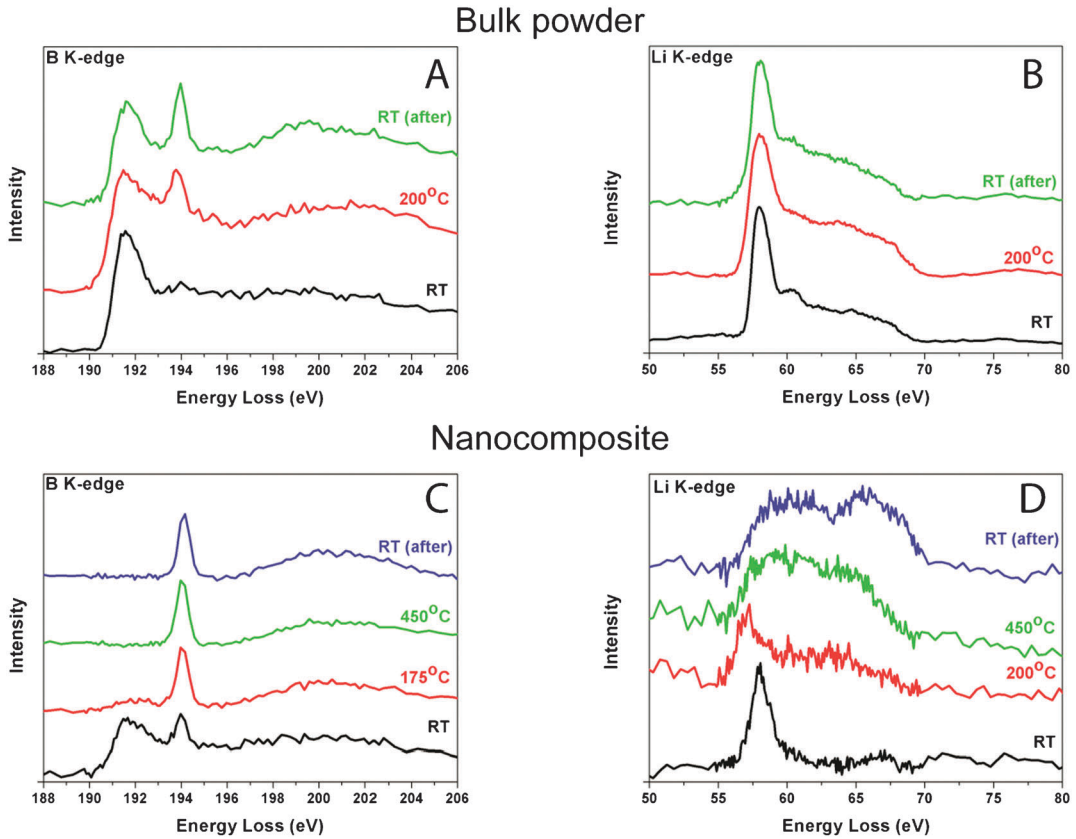

Fig. 3 (A and B) B K-edge XRS (A) and Li K-edge (B) XRS of bulk $LiBH_4$ powder at room temperature (RT, bottom line), at 200 °C (200 °C, line in the middle) and at RT after being at 200 °C (RT (after), top line); C and D) B K-edge XRS (C) and Li K-edge XRS (D) of nano-composite $LiBH_4$/C at room temperature (RT, bottom line), at 175 °C, at 450 °C and after the treatment at room temperature (RT (after), top line).

the boron is oxidized. A single peak at 194 eV distinguishes from the calculated XAS spectra of LiB, LiBH and $Li_2B_{12}H_{12}$ and B(tetragonal), where also intensity close to 194 eV can be found, but then also other peaks at different energies should be visible. The Li K-edge XRS of $LiBH_4$/C (Fig. 3D) changes completely going from room temperature to higher temperatures. The Li K-edge XRS at room temperature looks rather similar to the Li K-edge XRS of bulk $LiBH_4$. Li K-edge spectra at higher temperatures have two broader peaks, which could correspond to lithium atoms intercalated in the carbon structure as previously reported.[42] The Li XAS of intercalated lithium atoms into carbon (LiC_6) has two broad peaks in the 62–70 eV range.[43] An alternative explanation of the peaks is the formation of $Li_xO_yH_z$[37,44] or $LiBO_2$, as it was recently reported that $NaBO_2$ can be formed in the case of nanoconfined $NaBH_4$.[45]

D Rehydrogenation of nanoconfined $LiBH_4$

The B K-edge spectra of $LiBH_4$/C as prepared and the rehydrogenated $LiBH_4$/C are shown in Fig. 4A. The as prepared and rehydrogenated spectra resemble each other, which indicates that the hydrogen desorption from the nanoconfined $LiBH_4$ is reversible and that the electronic structure of the as prepared sample is largely regained after rehydrogenation.

E Carbon K-edge measurements

In Fig. 4C and D, C K-edge XRS spectra are shown for physical mixtures of $LiBH_4$ and graphite (Fig. 4C) and porous carbon (Fig. 4D) There are differences for graphite and porous carbon: in Fig. 4C the C K-edge XRS does not differ in the as prepared and dehydrogenated case, so the graphite carbon does not play a role in the (stabilization of the) dehydrogenation process. The spectrum of a physical mixture of $LiBH_4$ and porous carbon shows a clear difference between the as prepared and the dehydrogenated sample (Fig. 4D). A peak appears at approximately 291 eV as indicated with the arrow. This peak might indicate a carbon that is bound to oxygen. The C K-edge XRS of $LiBH_4$/C as prepared by melt infiltration (bottom line, as prep.), dehydrogenated (dehydr.) and rehydrogenated (rehydr.) are shown in Fig. 4B. The C K-edge XRS of $LiBH_4$/C as prepared and after dehydrogenation are different. The peak at the same spot at 291 eV as in Fig. 4D comes up. The peak shift in the present case (−1.3 eV) is different from the −0.6 eV as reported by Balasubramanian *et al.*,[43] thus it cannot be directly attributed to lithium intercalation. The C K-edge XRS of the as prepared physically mixed $LiBH_4$ and porous carbon with the $LiBH_4$/C confirm that the nature of the carbon does not change by the melt infiltration procedure. An additional remark is that the morphology of the porous and non-porous carbon materials is different.

The Li K-edge XRS in Fig. 3D for $LiBH_4$ after dehydrogenation (RT (after), top line) has features that correspond to the Li K-edge of LiC_6 as reported by Balasubramanian *et al.*[43] This has the effect of stabilization of the dehydrogenation products of $LiBH_4$ and hence facilitation, by lowering

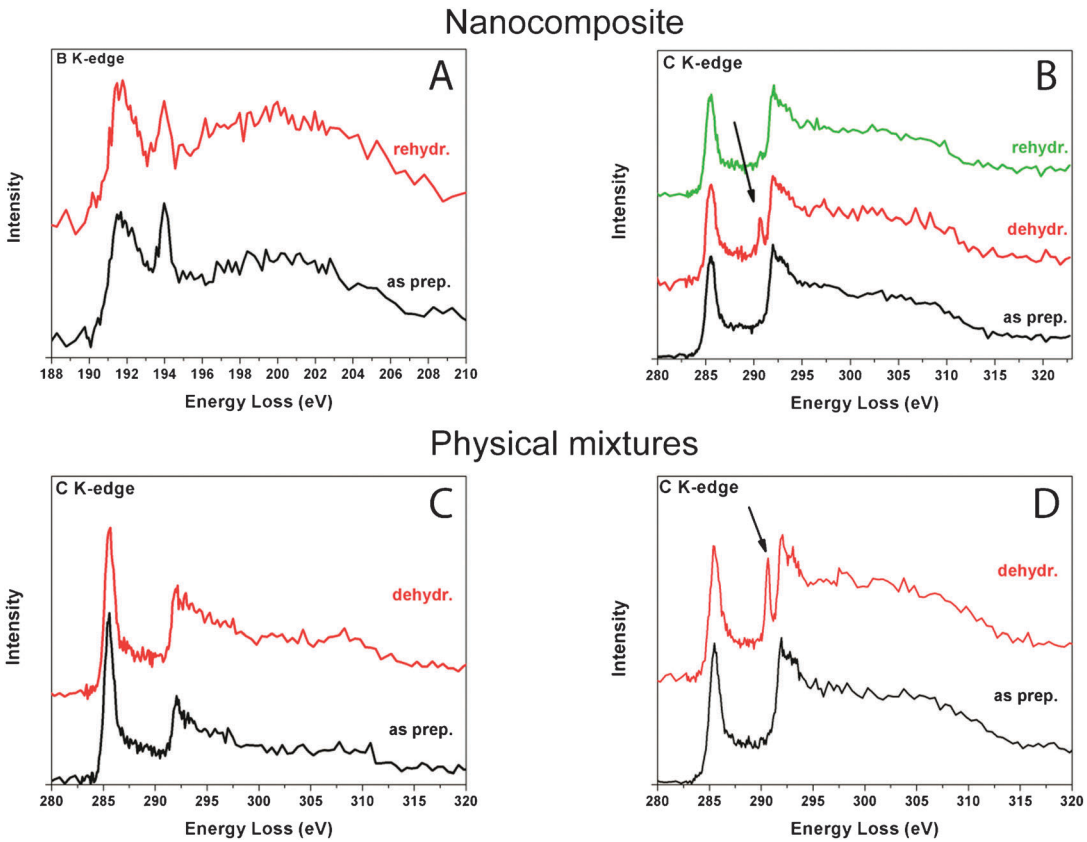

Fig. 4 (A) B K-edge XRS comparison at room temperature of $LiBH_4$/C as prepared (as prep., bottom line) with a sample that has been dehydrogenated and subsequently rehydrogenated (rehydr., top line) again. (B) C K-edge XRS spectra at room temperature of $LiBH_4$/C as prepared (as prep., bottom line), after dehydrogenation (dehydr., line in the middle) and rehydrogenation (rehydr., top line). (C and D) C K-edge XRS spectra at room temperature of physical mixtures of (C) $LiBH_4$ and graphite as prepared (as prep., bottom line) and after dehydrogenation (dehydr., top line); (D) $LiBH_4$ and porous carbon as prepared (as prep., bottom line) and after dehydrogenation (dehydr., top line).

the enthalpy change (ΔH), for dehydrogenation. The rehydrogenated $LiBH_4$/C sample has an XRS spectrum that is the same as the XRS spectrum of the $LiBH_4$/C as prepared. This confirms that the electronic structure of the nanoconfined $LiBH_4$ is largely regained by rehydrogenation. Note that XRS cannot give proof for the fraction that can be rehydrogenated.

The samples under investigation show an oxygen contamination. Due to the oxygen cleaning ability of the materials under study, which means that these materials will pick up any (scarce) amount of oxygen in the environment, it is almost unavoidable to get rid of oxygen contamination that we observe. The most likely source of oxygen is the oxygen that is created upon heating of the steel chamber, which is unavoidable in the present experiment. Note that the amounts of oxygen contamination are not clear, since the B K-edge peak at 194 eV is very intense, so even visible for small oxygen contaminations. This investigation shows that differences in the electronic structure during dehydrogenation and after rehydrogenation can be obtained using XRS. However, due to circumstances we did not find a clear proof for the intermediates during dehydrogenation. This could mean that the electronic structure changes are not too clear from XRS, although we could observe a slight broadening of the first peak in the B K-edge after dehydrogenation.

One important improvement would be the energy resolution. If the energy resolution is improved, the differences and therefore the possible intermediate states would be much clearer.

4 Conclusions

In this article we have shown XRS spectra of bulk $LiBH_4$ and nanoconfined $LiBH_4$/C. With the XRS technique, changes in the electronic structure during dehydrogenation and after rehydrogenation of the separate elements lithium, boron and carbon can be studied. Unfortunately oxygen-containing compounds were detected. The sample handling needs to be optimized. Nevertheless, it was found that the electronic structure of the rehydrogenated samples was confirmed to be the same as the as prepared samples, which means that the expected reversibility, which was based on the bulk $LiBH_4$ and NMR results,[9] was in this paper found on the basis of a technique that does not need crystalline materials. The major advantage of XRS measurements is that one can measure the Li and B K edges with hard X-rays, allowing *in situ* experiments that are not feasible with direct XAS measurements.

This study showed that *in situ* XRS experiments in combination with calculations are a promising tool to study the electronic properties of nano-crystalline or nano-sized non-crystalline lightweight materials for energy storage. In the future, we hope to

study more relevant reference systems and find the route of de- and re-hydrogenation for both the bulk $LiBH_4$ and nano-confined $LiBH_4$/C.

Acknowledgements

The Stanford Synchrotron Radiation Lightsource is a National User Facility operated by Stanford University on behalf of the U.S. Department of Energy, Office of Basic Energy Sciences. Matteo Calandra is acknowledged for providing the B and Li pseudopotentials with and without a (half) core-hole. PSM and FMFdG acknowledge NWO-CW/Vici for financial support. PN and PEdJ acknowledge NWO-CW/Vidi 016.072.316 for financial support. Timcal Switzerland is acknowledged for the provision of the graphite and porous carbon.

References

1 E. de Smit, I. Swart, J. F. Creemer, G. H. Hoveling, M. K. Gilles, T. Tyliszczak, P. J. Kooyman, H. W. Zandbergen, C. Morin, B. M. Weckhuysen and F. M. F. de Groot, *Nature*, 2008, **456**, 222–225.
2 J. F. Creemer, S. Helveg, G. H. Hoveling, S. Ullmann, A. M. Molenbroek, P. M. Sarro and H. W. Zandbergen, *Ultramicroscopy*, 2008, **108**, 993–998.
3 A. Knop-Gericke, M. Hävecker, T. Neisius and T. Schedel-Niedrig, *Nucl. Instrum. Methods Phys. Res., Sect. A*, 1998, **406**, 311–322.
4 F. M. F. de Groot, M. A. Arrio, P. Sainctavit, C. Cartier and C. T. Chen, *Solid State Commun.*, 1994, **92**, 991–995.
5 M. Krisch and F. Sette, *Surf. Rev. Lett.*, 2002, **9**, 969–976.
6 M. H. Krisch, F. Sette, C. Masciovecchio and R. Verbeni, *Phys. Rev. Lett.*, 1997, **78**, 2843–2846.
7 U. Bergmann, P. Glatzel and S. P. Cramer, *Microchem. J.*, 2002, **71**, 221–230.
8 A. Züttel, P. Wenger, S. Rentsch, P. Sudan, P. Mauron and C. Emmenegger, *J. Power Sources*, 2003, **118**, 1–7.
9 S.-I. Orimo, Y. Nakamori, N. Ohba, K. Miwa, M. Aoki, S. Towata and A. Züttel, *Appl. Phys. Lett.*, 2006, **89**, 021920.
10 S.-J. Hwang, R. C. Bowman Jr., J. W. Reiter, J. Rijssenbeek, G. L. Soloveichik, J.-C. Zhao, H. Kabbour and C. C. Ahn, *J. Phys. Chem. C*, 2008, **112**, 3164–3169.
11 R. Caputo and A. Zuttel, *Mol. Phys.*, 2010, **108**, 1263–1276.
12 J. K. Kang, S. Y. Kim, Y. S. Han, R. P. Muller and W. A. Goddard III, *Appl. Phys. Lett.*, 2005, **87**, 1–3.
13 N. Ohba, K. Miwa, M. Aoki, T. Noritake, S.-I. Towata, Y. Nakamori, S.-I. Orimo and A. Züttel, *Phys. Rev. B: Condens. Matter*, 2006, **74**, 075110.
14 P. Adelhelm and P. E. de Jongh, *J. Mater. Chem.*, 2011, **21**, 2417–2427.
15 P. E. de Jongh and P. Adelhelm, *ChemSusChem*, 2010, **3**, 1332–1348.
16 A. F. Gross, J. J. Vajo, S. L. Van Atta and G. L. Olson, *J. Phys. Chem. C*, 2008, **112**, 5651–5657.
17 P. Ngene, R. Van Zwienen and P. E. de Jongh, *Chem. Commun.*, 2010, **46**, 8201–8203.
18 M. Vaarkamp, B. L. Mojet, M. J. Kappers, J. T. Miller and D. C. Koningsberger, *J. Phys. Chem.*, 1995, **99**, 16067–16075.
19 W. M. Heijboer, D. C. Koningsberger, B. M. Weckhuysen and F. M. F. de Groot, *Catal. Today*, 2005, **100**, 228.
20 W. Schülke and H. Nagasawa, *Nucl. Instrum. Methods Phys. Res.*, 1984, **222**, 203–206.
21 K. Hämäläinen, S. Manninen, C.-C. Kao, W. Caliebe, J. B. Hastings, A. Bansil, S. Kaprzyk and P. M. Platzman, *Phys. Rev. B: Condens. Matter*, 1996, **54**, 5453–5459.
22 R. S. Pease, *Acta Crystallogr.*, 1952, **5**, 356–361.
23 WWW-MINCRYST (2011), http://database.iem.ac.ru/mincryst.
24 http://www.oxmat.co.uk/Crysdata/lih.htm.
25 J.-H. Her, M. Yousufuddin, W. Zhou, S. S. Jalisatgi, J. G. Kulleck, J. A. Zan, S.-J. Hwang, R. C. Bowman Jr. and T. J. Udovic, *Inorg. Chem.*, 2008, **47**, 9757–9759.
26 H. Effenberger, C. L. Lengauer and E. Parthe, *Monatsh. Chem.*, 2001, **132**, 1515–1517.
27 P. Giannozzi, S. Baroni, N. Bonini, M. Calandra, R. Car, C. Cavazzoni, D. Ceresoli, G. L. Chiarotti, M. Cococcioni, I. Dabo, A. Dal Corso, S. De Gironcoli, S. Fabris, G. Fratesi, R. Gebauer, U. Gerstmann, C. Gougoussis, A. Kokalj, M. Lazzeri, L. Martin-Samos, N. Marzari, F. Mauri, R. Mazzarello, S. Paolini, A. Pasquarello, L. Paulatto, C. Sbraccia, S. Scandolo, G. Sclauzero, A. P. Seitsonen, A. Smogunov, P. Umari and R. M. Wentzcovitch, *J. Phys.: Condens. Matter*, 2009, **21**, 395502.
28 C. Gougoussis, M. Calandra, A. Seitsonen, C. Brouder, A. Shukla, F. Mauri, ArXiv:0806.4706v1, 2008.
29 C. Gougoussis, M. Calandra, A. P. Seitsonen and F. Mauri, *Phys. Rev. B: Condens. Matter*, 2009, **80**, 075102.
30 M. Taillefumier, D. Cabaret, A.-M. Flank and F. Mauri, *Phys. Rev. B: Condens. Matter*, 2002, **66**, 1951071–1951078.
31 J. A. McLeod, R. G. Wilks, N. A. Skorikov, L. D. Finkelstein, M. Abu-Samak, E. Z. Kurmaev and A. Moewes, *Phys. Rev. B: Condens. Matter*, 2010, **81**, 245123.
32 V. Mauchamp, M. Jaouen and P. Schattschneider, *Phys. Rev. B: Condens. Matter*, 2009, **79**, 235106.
33 S.-P. Gao, C. J. Pickard, M. C. Payne, J. Zhu and J. Yuan, *Phys. Rev. B: Condens. Matter*, 2008, **77**, 115122.
34 C. Brouder, *J. Phys.: Condens. Matter*, 1990, **2**, 701–738.
35 D. Li, G. M. Bancroft, M. E. Fleet, P. C. Hess and Z. F. Yin, *Am. Mineral.*, 1995, **80**, 873–877.
36 C.-G. Lee, H.-J. Sohn and M. G. Kim, *Solid State Ionics*, 2005, **176**, 1237–1241.
37 S. K. Lee, P. J. Eng, H.-k. Mao, Y. Meng and J. Shu, *Phys. Rev. Lett.*, 2007, **98**, 105502.
38 R. Arenal, F. de la Peña, O. Stéphan, M. Walls, M. Tencé, A. Loiseau and C. Colliex, *Ultramicroscopy*, 2008, **109**, 32–38.
39 S.-P. Gao, C. J. Pickard, A. Perlov and V. Milman, *J. Phys.: Condens. Matter*, 2009, **21**, 104203.
40 D. N. Jayawardane, C. J. Pickard, L. M. Brown and M. C. Payne, *Phys. Rev. B: Condens. Matter*, 2001, **64**, 1151071–1151074.
41 A. Mattila, J. A. Soininen, S. Galambosi, S. Huotari, G. Vankó, N. D. Zhigadlo, J. Karpinski and K. Hämäläinen, *Phys. Rev. Lett.*, 2005, **94**, 1–4.
42 P. Ngene, M. H. W. Verkuijlen, Q. Zheng, J. Kragten, P. J. M. van Bentum, J. H. Bitter and P. E. de Jongh, *Faraday Discuss.*, 2011, **151**, 47–58.
43 M. Balasubramanian, C. S. Johnson, J. O. Cross, G. T. Seidler, T. T. Fister, E. A. Stern, C. Hamner and S. O. Mariager, *Appl. Phys. Lett.*, 2007, **91**, 031904.
44 J. Tsuji, H. Nakamatsu, T. Mukoyama, K. Kojima, S. Ikeda and K. Taniguchi, *X-Ray Spectrom.*, 2002, **31**, 319–326.
45 P. Ngene, R. Van Den Berg, M. H. W. Verkuijlen, K. P. De Jong and P. E. de Jongh, *Energy Environ. Sci.*, 2011, **4**, 4108–4115.